

Viscoelastic model for bending process of continuous fiber-reinforced thermoplastic sheets

M. T. ABADI

*Aerospace Research Institute, Ministry of Science, Research and Technology,
Tehran, Iran, e-mail: abadi@ari.ac.ir*

THIS PAPER PRESENTS AN ANALYSIS OF THE BENDING PROCESS in thermoplastic sheets reinforced with unidirectional continuous fibers. To capture the material's viscoelastic response during the bending process, a novel viscoelastic model is described based on the concept of transient reversible networks. The model incorporates kinematic constraints of material incompressibility and fiber inextensibility during deformation of the composite sheets. An analytical solution is derived, enabling the determination of the deformed geometry and bending forces as time-dependent functions of the bending angle, the deformation rate, and material parameters. The model's performance is evaluated through comparisons with existing experimental data and a prior viscous model for bending process at various deformation rates. This comparison aids in identifying the material parameters and characteristic time associated with the transient reversible networks.

Key words: fiber-reinforced composite, viscoelastic, stresses relaxation, forming.



Copyright © 2025 The Author.

Published by IPPT PAN. This is an open access article under the Creative Commons Attribution License CC BY 4.0 (<https://creativecommons.org/licenses/by/4.0/>).

1. Introduction

THE FORMABILITY OF THERMOPLASTIC SHEETS reinforced with continuous fibers plays a critical role in their design and manufacturing processes. During the forming process, the thermoplastic matrix undergoes a melting transition, allowing the reinforcing fibers to conform to the die geometry. Subsequently, after shaping the composite sheet to the desired geometry, it is cooled to solidify the melted resin and fix the fibers in their deformed configuration before load removal. This process significantly influences the forming force required, which depends on factors such as the magnitude and rate of deformation, as well as the processing temperature [1, 2]. Unfortunately, forming processes can result in various defects in the final parts, including sheet wrinkling, fiber buckling, fiber rupture, and excessive resin percolation [3–6]. Optimizing processing parameters is essential to achieve the desired final shape while minimizing defects. Previous studies have investigated the underlying causes of these defects through experimental investigations [2–4] and numerical analyses [7–9].

Some anisotropic viscous constitutive laws have been presented to model the response of the continuous fiber-reinforced thermoplastic sheets at the forming temperature [10, 11]. The high ratio of bulk to shear viscosity in melted resin is given [12], the deformation of the composite sheets is assumed to be incompressible. Additionally, the presence of continuous fibers within the melted resin significantly restricts deformation and introduces inextensible directions throughout the composite [3, 13]. The micromechanical technique has been employed to characterize the rheological properties of viscous fluids reinforced with unidirectional continuous fibers [14]. This study demonstrates that the response of such composites in transverse intraply shear and squeeze flows depends on both the deformation history and the rate of deformation.

Several numerical procedures have been developed to analyze the sheet forming process using viscous models while incorporating the relevant kinematic constraints [15–18]. However, these models exhibit limitations due to the dependence of the viscous stress tensor on the rate-of-deformation tensor. This dependence leads to a discontinuous jump in the calculated forming force at the initiation of deformation for a constant deformation rate. Additionally, viscous models predict a zero-force required to maintain a constant deformation in thermoplastic composites, which contradicts experimental observations. Experimental studies have demonstrated that for thermoplastic composites undergoing the constant rate deformation, the forming force continuously increases from zero at the initial instant [19–21]. Furthermore, the force required to maintain a constant deformation exhibits stress relaxation, continuously decaying to a specific value over a sufficiently long time after the forming process ceases [19–21]. Therefore, viscous models are demonstrably incapable of accurately predicting the mechanical response of reinforced thermoplastic sheets at the forming temperature. While some prior research has explored using an equivalent elastic material for the melted resin [22, 23], these models can account for the dependence of the stress field on the amount of deformation. However, they fail to capture the rate-dependent response and stress relaxation observed in experimental studies [19–21]. A viscoelastic model is thus the ideal choice for simulating the forming process of thermoplastic composites at elevated temperatures.

Finite strain anisotropic viscoelastic constitutive laws can handle large deformations and the nonlinear material behavior more effectively. This leads to more accurate predictions of the final part shape, residual stresses, and potential defects, improving the process design and part quality. Viscoelastic models can capture the time-dependent behavior of thermoplastic composites at elevated temperatures, crucial for accurately predicting the material’s response during the thermoforming process. GUZMAN-MALDONADO *et al.* [24] proposed a visco-hyperelastic model to simulate the thermoforming process of thermoplastic prepregs. This model combines the advantages of both viscoelastic and hy-

perelastic models, the latter of which can capture large deformations and nonlinear elastic behavior. Their viscoelastic models have primarily focused on intra-ply shear deformation, neglecting the significant viscoelastic effects observed in inter-ply shear deformations, such as those encountered in the bending forming of laminated composite sheets [19–21]. SÁNCHEZ *et al.* [25] used a generalized Maxwell model to simulate the thermoforming process of polystyrene. The generalized Maxwell model is a viscoelastic model consisting of a series of spring-dashpot elements, each representing a different relaxation time. The relaxation functions were directly applied on two linear elastic constants including shear module and bulk module. HOLZAPFEL and GASSER [26] developed a viscoelastic model for fiber-reinforced composites at finite strains. Previous studies have modeled the relaxation and/or creep response of individual composite constituents and assembled their contributions to obtain a global response. DÖRR *et al.* [28] modeled the bending process of thermoplastic materials reinforced with unidirectional fibers or woven/bidirectional fabric using a viscoelastic constitutive law. They assumed an additive decomposition of stress tensor into a purely elastic stress and the internal viscoelastic stress defined by the generalized Maxwell or the Voigt–Kelvin approach. A hypoelastic constitutive law was used to model the purely elastic stress. The combination of hypoelastic model with Voigt–Kelvin model captures the immediate elastic response and delayed viscous response, while its combination with a generalized Maxwell model accounts for multiple relaxation times. CHEN *et al.* [27] proposed a viscoelastic model for fiber-reinforced composites at finite deformations. They employed a homogenization framework to decompose the Helmholtz free energy density function of each constituent (matrix and fiber) into volumetric, isochoric, and dissipative parts. An effective evolution rule was developed to govern the time-dependent, viscous behavior of each composite phase. The long-term (purely elastic) behaviors of both the matrix and the fibers were characterized by the incompressible neo-Hookean model. The elastic free energy density functions of the matrix and the fibers were derived based on a specific multiplicative decomposition of the deformation gradient. NEDJAR [29] presented an anisotropic viscoelastic constitutive law that treats the matrix and the fibers separately. The relaxation and/or creep response of each constituent was derived based on a multiplicative viscoelastic split of the deformation gradient, combined with the assumption of viscoelastic potentials. This approach allows for the accurate representation of the time-dependent, anisotropic behavior of the composite material under various loading conditions. TAGILTSEV *et al.* [30] used a multiplicative approach to simulate the viscoelastic properties of a composite material. They introduced a new family of hyperelastic potentials to account for local compressive fiber buckling. This approach allows for the accurate representation of the nonlinear, time-dependent behavior of the composite material under complex loading conditions.

This research presents an anisotropic viscoelastic model, based on the Transient Network Theory (TNT), to analyze the mechanical response of unidirectional continuous fiber-reinforced thermoplastic sheets during bending, incorporating both intra-ply and inter-ply shear deformations. Unlike previous studies that treated the matrix and fibers separately, a continuum approach is employed to model the composite media, neglecting porosity formation and resin percolation. The composite sheet is modeled as a transversely isotropic viscoelastic material, constrained by fiber inextensibility and material incompressibility. The presence of active links in the reversible networks necessitates a reinforced hyperelastic material model within the continuum approach to accommodate finite deformations. The hyperelastic model is more suitable than the previous linear elastic model for simulating the large deformations experienced by composite laminates during thermoforming processes. The strain energy function for the hyperelastic material is formulated, adhering to principles of objectivity and material symmetry, and satisfying conditions of zero energy and stress in the reference configuration, while enforcing fiber inextensibility and material incompressibility. This research develops a general viscoelastic model that avoids multiplicative decomposition of the deformation gradient tensor and additive decomposition of the stress tensor. This model, within the TNT framework, evaluates both relaxation and creep responses using a single continuum approach.

The thermoforming simulation of composite sheets requires accurate material properties in different forming parameters. Some experimental procedures have been developed to determine material properties in different deformation modes, temperatures and deformation rates [31, 32]. Out-of-plane bending is one of the deformation mechanisms that govern the appearance of wrinkles during the thermoforming process [33]. Therefore, simulation of the bending process of reinforced thermoplastic laminates provides information for predominate material characteristics. Previous research works simulated the bending process to determine the parameters of a viscous model, while the present research work focuses on the determination of the material parameter in a finite viscoelastic model by analyzing the bending process of thermoplastic composites at elevated temperatures.

The viscoelastic model developed in the present research work is employed to analyze bending and derive an analytical solution. This solution determines the deformed geometry and forces required to bend the composite sheets and maintain a specific deformation state. These forces are presented as time-dependent functions of the bending angle, rate of deformation, and material parameters. The model not only describes the material response during bending but also captures the stress relaxation phenomenon for a prescribed deformed configuration. By comparing the analytical solution with previous experimental results [19], this work establishes a method to determine the material parameters and char-

acteristic time associated with the transient reversible networks. Furthermore, the viscoelastic model is evaluated for bending processes with varying deformation rates. The analytical results are compared with both prior experimental data and predictions from the aforementioned viscous model.

2. Viscoelastic model

Drawing upon the theory of transient reversible networks [23, 34], this work proposes an incompressible anisotropic viscoelastic model for thermoplastic sheets reinforced with continuous inextensible fibers. The polymer resin is modeled as a network of interconnected molecular chains, as illustrated in Fig. 1. An active chain, defined as a chain with both ends attached to distinct junctions, is represented by a nonlinear elastic spring. The rupture of a bond at a chain terminus is considered equivalent to chain scission. When a dangling chain (a chain with one free end shown in Fig. 1) encounters and captures a neighboring junction, a new adaptive link is formed. It is postulated that the characteristic timescale of the system, which is the time scale associated with the overall network dynamics, significantly exceeds the relaxation time of stress within a broken bond. Consequently, a dangling chain is assumed to be fully relaxed before capturing a new junction.

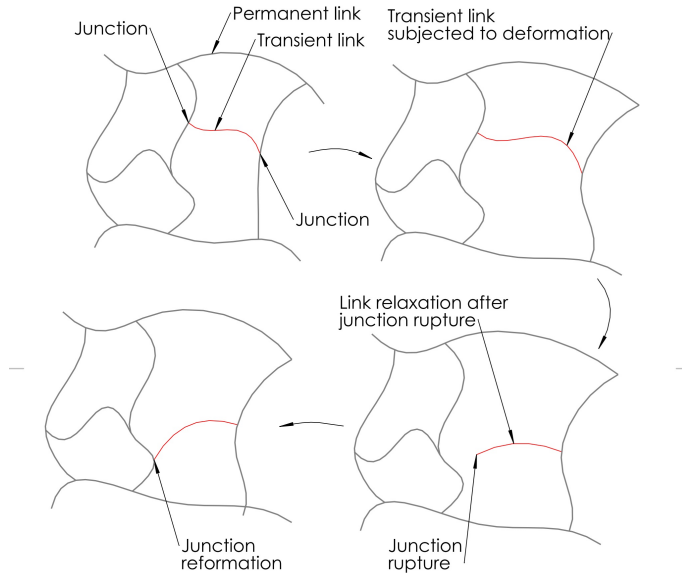


FIG. 1. Schematic illustration of the deformation-induced rupture and reformation of transient links in a polymer network.

The molten thermoplastic resin within the composite material is conceptualized as a network comprised of K distinct types of links. The number of each link type is determined with respect to a unit volume of the reference configuration. Initially, at time $t = 0$, the network is composed of $Y_k(0, 0)$ active links of type k . The number of initial links existing at time t is designated by $Y_k(t, 0)$. Some active links never break during deformation process of viscoelastic materials. The permanent links of type k are quantified by $\chi_k Y_k(0, 0)$, in which χ_k is the relative fraction of permanent links. In addition to, $Y_k(t, \tau)$ is the number of links arising before time instant τ and existing at time t . The number of links arisen within the interval $[\tau, \tau + d\tau]$ and existing at an instant t is determined by $(\partial Y_k(t, \tau)/\partial \tau)d\tau$. Hence, the total active links at instant t can be given by

$$(2.1) \quad Y(t) = \sum_{k=1}^K \left[Y_k(t, 0) + \int_0^t (\partial Y_k(t, \tau)/\partial \tau) d\tau \right].$$

This study investigates the application of various interconnection types within a reversible transient network model. This model aims to capture the viscoelastic behavior, characterized by complex stress relaxation responses, observed in diverse thermoplastic resins reinforced with continuous fibers. The composite materials are assumed to exhibit non-aging viscoelastic behavior, where the total number of active links remains constant, and the rate of link reformation is constant. In non-aging materials, the number of broken links depends on the difference between the current and reformation instants. Consequently, the functions of $Y_k(t, 0)$ and $\partial Y_k(t, \tau)/\partial \tau$ can be expressed as [35, equations 3.2 and 3.140]:

$$(2.2) \quad Y_k(t, 0) = Y_k(0, 0)[\chi_k + (1 - \chi_k) \exp(-\Gamma_k t)],$$

$$(2.3) \quad \partial Y_k(t, \tau)/\partial \tau = Y_k(0, 0)\Gamma_k(1 - \chi_k) \exp[-\Gamma_k(t - \tau)],$$

where Γ_k represents the reformation rate of active links.

The strain energy at the current instant is the sum of the stored energy in the initial active links and the reformed links during the deformation process [36], namely,

$$(2.4) \quad w(t) = \sum_{k=1}^K \left[Y_k(t, 0)w_k(t, 0) + \int_0^t (\partial Y_k(t, \tau)\partial \tau)w_k(t, \tau) d\tau \right].$$

To assess the response of the network, which consists of multiple active links, the strain energy stored within all active links at a specific time instant needs to be determined. Due to the presence of these active links, the composite material undergoing finite deformation can be considered a reinforced hyperelastic material in the continuum approach.

The strain energy function must satisfy the following criteria: objectivity, principle of material symmetry, and the conditions of zero energy and zero stress in the reference configuration. The objectivity condition is satisfied by expressing the strain energy in terms of the right Cauchy–Green deformation tensor, which is symmetric and positive definite. Additionally, the material symmetry condition necessitates that the function remains invariant under transformations involving elements of the material symmetry group. The strain energy function is chosen to be polyconvex. This ensures physically realistic material responses and guarantees the existence and stability of solutions for boundary value problems [37–39]. The strain energy function is derived within the context of the invariant theory, utilizing the structural tensors. It satisfies both polyconvexity and coercivity conditions.

A hyperelastic material reinforced with unidirectional continuous fibers can be described by a strain energy density function, $w(\mathbf{F}, \mathbf{a})$, in terms of the deformation gradient tensor, \mathbf{F} , and the unit vector, \mathbf{a} , along the fiber at the time of link formation [28]. The fibers are modeled as material lines. This allows us to determine their current direction using the deformation gradient tensor and the initial fiber direction. The energy function must satisfy the objectivity condition and the principle of material symmetry. Representing the strain energy as a function of invariants derived from the right Cauchy–Green deformation tensor, $\mathbf{C} = \mathbf{F}^T \mathbf{F}$, and the unit vector, inherently ensures that it fulfills both the objectivity condition and the principle of material symmetry. Based on the theory of representations for scalar-valued tensor functions [40], the strain energy density function per unit volume of the reference configuration can be expressed as $w_k(I_1, I_2, I_3, I_4, I_5)$, where the invariants I_i are expressed as:

$$(2.5a) \quad I_1(t, \tau) = \text{tr } \mathbf{C}(t, \tau),$$

$$(2.5b) \quad I_2(t, \tau) = [(\text{tr } \mathbf{C}(t, \tau))^2 - \text{tr } \mathbf{C}^2(t, \tau)]/2,$$

$$(2.5c) \quad I_3(t, \tau) = \det \mathbf{C}(t, \tau),$$

$$(2.5d) \quad I_4(t, \tau) = \mathbf{C}(t, \tau) : \mathbf{A}(\tau),$$

$$(2.5e) \quad I_5(t, \tau) = \mathbf{C}^2(t, \tau) : \mathbf{A}(\tau),$$

where $\mathbf{A}(\tau)$ is a symmetric second order tensor with the components of $A_{ij}(\tau) = a_i(\tau)a_j(\tau)$. The definition of polyconvexity necessitates that the invariants considered as arguments of the strain energy function exhibit convex properties [41]. The convexity of each invariant can be demonstrated by examining the positivity of the second derivative. Specifically, it can be established that the invariants I_1 , I_2 , I_3 and I_4 are convex with respect to \mathbf{F} , $\text{Cof}(\mathbf{F})$, $\det(\mathbf{F})$ and \mathbf{F} , respectively. However, the invariant I_5 is not convex with respect to \mathbf{F} [42]. SCHRÖDER *et al.* [42] derived a convex mixed invariant using the Cayley–Hamilton theorem as follows:

$$(2.6) \quad K_5(t, \tau) = \text{Cof}(\mathbf{C}(t, \tau)) : \mathbf{A}(\tau) = I_5(t, \tau) - I_4(t, \tau)I_1(t, \tau) + I_2(t, \tau).$$

Thus, the polyconvexity condition is met by expressing the strain energy as a function of invariants I_1, I_2, I_3, I_4, K_5 , denoted as $w_k(I_1, I_2, I_3, I_4, K_5)$. A polyconvex function can be decomposed into isotropic and anisotropic parts under different loading conditions [41, 43, 44], i.e.,

$$(2.7) \quad w_k(t, \tau) = \hat{w}_k^{\text{iso}}(I_1(t, \tau), I_2(t, \tau), I_3(t, \tau)) \\ + \hat{w}_k^{\text{aniso}}(I_3(t, \tau), I_4(t, \tau), K_5(t, \tau)).$$

Due to the kinematical constraints of material incompressibility and fiber inextensibility, the invariants I_3 and I_4 take on unit values, respectively. Consequently, the strain energy function simplifies to:

$$(2.8) \quad w_k(t, \tau) = \hat{w}_k^{\text{iso}}(I_1(t, \tau), I_2(t, \tau), 1) + \hat{w}_k^{\text{aniso}}(1, 1, K_5(t, \tau)) \\ = w_k^{\text{iso}}(I_1(t, \tau), I_2(t, \tau)) + w_k^{\text{aniso}}(K_5(t, \tau)).$$

For a reversible network containing K distinct types of links, the total strain energy can be expressed as:

$$(2.9) \quad w(t) = \sum_{k=1}^K \left\{ Y_{k(t,0)} [w_k^{\text{iso}}(I_1(t,0), I_2(t,0)) + w_k^{\text{aniso}}(K_5(t,0))] \right. \\ \left. + \int_0^t (\partial Y_{k(t,\tau)} / \partial \tau) [w_k^{\text{iso}}(I_1(t,\tau), I_2(t,\tau)) + w_k^{\text{aniso}}(K_5(t,\tau))] d\tau \right\}.$$

The kinematical constraints can be incorporated into the strain energy function using Lagrange multipliers, namely,

$$(2.10) \quad w_c(t) = Y_{(0,0)} [-p(I_3(t,0) - 1) + T(I_4(t,0) - 1)] + w(t),$$

where the functions $p(t)$ and $T(t)$ are Lagrange multipliers introduced to enforce the kinematical constraints of material incompressibility ($I_3 = 1$) and fiber inextensibility ($I_4 = 1$), respectively. The derivative of the strain energy with respect to the right Cauchy–Green deformation tensor yields the second Piola–Kirchhoff stress, i.e.,

$$(2.11) \quad \mathbf{S} = 2 \frac{\partial w}{\partial \mathbf{C}} = 2Y_{(0,0)} [-p\mathbf{C}^{-1} + T\mathbf{A}] \\ + \sum_{k=1}^K \left\{ Y_{k(t,0)} \left[\frac{\partial w_k^{\text{iso}}}{\partial I_1} \mathbf{I} + \frac{\partial w_k^{\text{iso}}}{\partial I_2} (I_1 \mathbf{I} - \mathbf{C}) + \frac{\partial w_k^{\text{aniso}}}{\partial K_5} (K_5 \mathbf{C}^{-1} - \mathbf{C}^{-1} \mathbf{A} \mathbf{C}^{-1}) \right] \right. \\ \left. + \int_0^t (\partial Y_{k(t,\tau)} \partial \tau) \left[\frac{\partial w_k^{\text{iso}}}{\partial I_1} \mathbf{I} + \frac{\partial w_k^{\text{iso}}}{\partial I_2} (I_1 \mathbf{I} - \mathbf{C}) + \frac{\partial w_k^{\text{aniso}}}{\partial K_5} (K_5 \mathbf{C}^{-1} - \mathbf{C}^{-1} \mathbf{A} \mathbf{C}^{-1}) \right] d\tau \right\}.$$

The energy-free and stress-free conditions are expressed as follows:

$$(2.12) \quad w_k^{\text{iso}}(3, 3) = w_k^{\text{aniso}}(1) = 0,$$

$$(2.13) \quad p(0) = \frac{\partial w_k^{\text{iso}}(3, 3)}{\partial I_1} + 2 \frac{\partial w_k^{\text{iso}}(3, 3)}{\partial I_2} + \frac{\partial w_k^{\text{aniso}}(1)}{\partial K_5},$$

$$(2.14) \quad T(0) = \frac{\partial w_k^{\text{aniso}}(1)}{\partial K_5}.$$

The isotropic part of strain energy is described using the Mooney–Rivlin model, while the corresponding anisotropic part is expressed as a linear model, namely,

$$(2.15) \quad w_k^{\text{iso}}(I_1(t, \tau), I_2(t, \tau)) = \frac{\beta_{k1}}{Y(0, 0)}(I_1(t, \tau) - 3) + \frac{\beta_{k2}}{Y(0, 0)}(I_2(t, \tau) - 3),$$

$$(2.16) \quad w_k^{\text{aniso}}(K_5(t, \tau)) = \frac{\beta_{k5}}{Y(0, 0)}(K_5(t, \tau) - 1),$$

where $Y_{(0,0)}$ is the number of the total active links and β_{ki} are the hyperelastic material parameters of the k -th kind active link. The considered models fulfill both the energy-free and stress-free conditions. Upon combining Eqs. (2.9), (2.15) and (2.16), the strain energy function can be expressed as:

$$(2.17) \quad w(t) = \sum_{k=1}^K \frac{Y_k(0, 0)}{Y(0, 0)} \left\{ [\chi_k + (1 - \chi_k) \exp(-\Gamma_k t)] \right. \\ \times [\beta_{k1}(I_1(t, 0) - 3) + \beta_{k2}(I_2(t, 0) - 3) + \beta_{k5}(K_5(t, 0) - 1)] \\ + \int_0^t (\Gamma_k(1 - \chi_k) \exp[-\Gamma_k(t - \tau)]) \\ \left. \times [\beta_{k1}(I_1(t, \tau) - 3) + \beta_{k2}(I_2(t, \tau) - 3) + \beta_{k5}(K_5(t, \tau) - 1)] d\tau \right\}.$$

3. Bending mechanism

A flat thermoplastic composite sheet is bent using a novel vee-bending mechanism developed in [19, 20]. The mechanism shown in Fig. 2a consists of a pair of rectangular plates hinged at the center of a loading roller (punch). These plates are supported on idler rollers with negligible friction. As the punch displaces vertically, the hinged plates rotate, pulling the composite sheet over the punch surface and inducing longitudinal shear deformation between layers. The experiment is conducted in a temperature-controlled environment, ensuring the composite sheet reaches equilibrium temperature before deformation. The punch

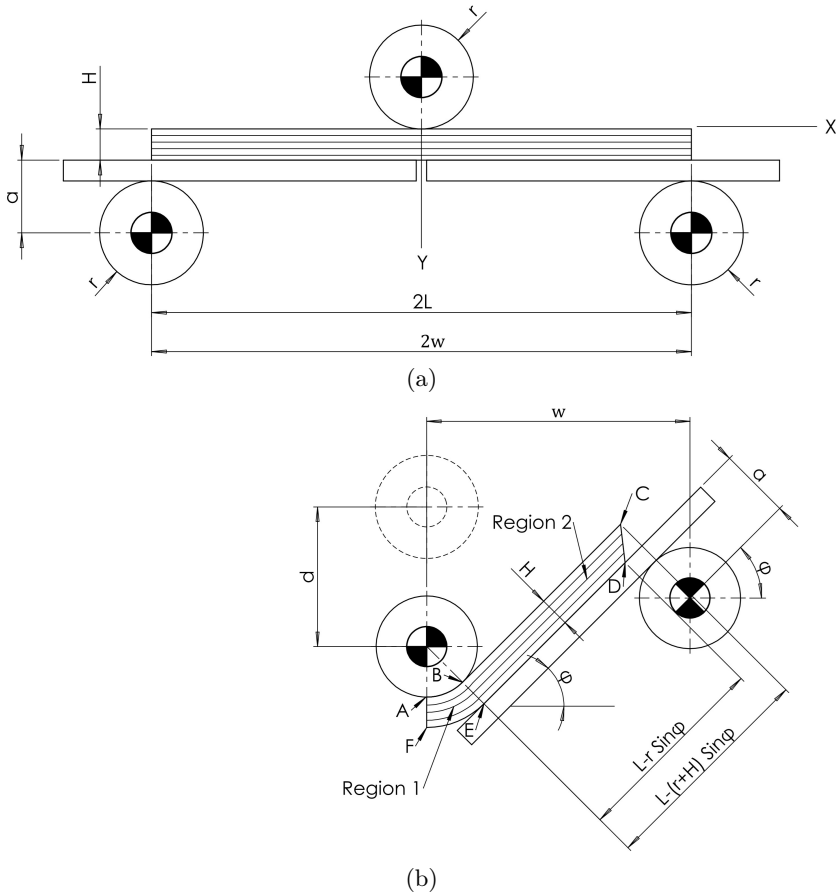


FIG. 2. Vee-bending mechanism (a) initial layout configuration (b) one half deformed configuration.

speed is maintained constant throughout the test, and the applied load is measured using a load cell. The bending process is terminated when the supporting plates reach a 45° rotation, corresponding to a 90° bending angle of the sample. The load cell also measures the force required to maintain this deformed geometry over time. To determine the net bending force, the force required to rotate the supporting plates and the sample weight are subtracted from the total measured load. A detailed description of the experimental procedure can be found in [19, 20]. The experimental results presented here serve to validate the analytical solution derived for the bending process.

Due to the high aspect ratio (width-to-thickness) of the bending sample, a state of plane strain deformation is assumed. The experimental samples possess unidirectional continuous fibers aligned parallel to the plane of deformation.

Previous research [45] has demonstrated that planar deformations in incompressible materials reinforced with inextensible fibers parallel to the deformation plane exhibit no thickness reduction. Consequently, intra-ply shear [46] becomes the dominant deformation mechanism in this configuration.

4. Bending deformation analysis

Figure 2b illustrates the deformation of the composite sample during the bending process. The reference configuration of the sample occupies the spatial domain defined by $-L \leq X \leq L$, $0 \leq Y \leq H$, and $-B \leq Z \leq B$, where $2L$, $2B$, and H represent the length, width, and thickness of the sample, respectively. Experimental studies [18, 19] have demonstrated negligible deformation in the Z -direction (out-of-plane) during bending. Due to the symmetry of the bending process about the punch centerline, analysis focuses on one half of the planar deformation. As depicted in Fig. 2b, the deformed geometry of the sample can be divided into two regions:

- Region 1 (ABEF) located at $0 \leq X \leq (r + Y)\phi(t) \leq Y \leq H$.
- Region 2 (BCDE) located at $(r + Y)\phi(t) \leq X \leq L \leq Y \leq H$.

The deformation of the two regions can be expressed as:

$$(4.1a) \quad \text{Region 1: } \begin{cases} x_{(X,Y,t)} = (r + Y) \sin \frac{X}{r+Y}, \\ y_{(X,Y,t)} = d - r + (r + Y) \cos \frac{X}{r+Y}, \end{cases}$$

$$(4.1b) \quad \text{Region 2: } \begin{cases} x_{(X,Y,t)} = (r + Y) \sin \phi(t) + [X - (r + Y)\phi(t)] \cos \phi(t), \\ y_{(X,Y,t)} = d - r + (r + Y) \cos \phi(t) \\ \quad - [X - (r + Y)\phi(t)] \sin \phi(t). \end{cases}$$

Given the geometric parameters r , a , and w depicted in Fig. 2, and the punch displacement d , the kinematical analysis establishes a relationship between the rotation angle (ϕ) of the supporting plates and the corresponding punch displacement (d) as follows:

$$(4.2) \quad (r + a + H)[1 - \sec \phi(t)] + w \tan \phi(t) - d = 0.$$

The invariants can be expressed using Eqs. (2.5), (2.6) and (4.1), i.e.,

$$(4.3a) \quad \text{Region 1: } I_{1(t)} - 3 = I_{2(t)} - 3 = K_{5(t)} - 1 = \left(\frac{X}{r + Y} \right)^2,$$

$$(4.3b) \quad \text{Region 2: } I_{1(t)} - 3 = I_{2(t)} - 3 = K_{5(t)} - 1 = \phi_{(t)}^2.$$

Equations (4.3) define the invariants of links that have been active since the initial time instant. To determine the invariants of links that reform at a specific instant, denoted by τ , and exist at a later time t , the right Cauchy–Green

deformation tensor is required. At a specific point within the material at time t , the components of the deformation gradient tensor are expressed as:

$$(4.4) \quad \frac{\partial x_i(t)}{\partial x_j(\tau)} = \frac{\partial x_i(t)}{\partial X_k} \frac{\partial X_k}{\partial x_j(\tau)},$$

X_k and $x_i(t)$ denote the Cartesian components of the material position vector in the reference configuration and the current configuration, respectively. Equation (4.4) can be written as:

$$(4.5) \quad \mathbf{F}_{(t,\tau)} = \mathbf{F}_{(t)} \mathbf{F}_{(\tau)}^{-1}.$$

According to Eq. (4.5), the deformation gradient of a link at the reformation time is the identity tensor ($\mathbf{F}_{(\tau,\tau)} = \mathbf{I}$), signifying no deformation. Subsequently, the total deformation gradient characterizes the link's deformation after the reformation time, which depends on both the total state and the configuration at the reformation time. Within the TNT framework, the links exhibit elastic behavior both before rupture and after reformation. Using Eq. (4.5), the right Cauchy–Green tensor at the current geometry for links reformed at instant τ can be expressed as:

$$(4.6) \quad \mathbf{C}_{(t,\tau)} = \mathbf{F}_{(t,\tau)}^T \mathbf{F}_{(t,\tau)} = \mathbf{F}_{(\tau)}^{-T} \mathbf{F}_{(t)}^T \mathbf{F}_{(t)} \mathbf{F}_{(\tau)}^{-1} = \mathbf{F}_{(\tau)}^{-T} \mathbf{C}_{(t)} \mathbf{F}_{(\tau)}^{-1}.$$

Based on the positions of a material point at the current and reformation instants (τ and t , respectively), three distinct cases are identified to determine the invariants of the right Cauchy–Green deformation tensor. These cases are categorized based on the point's location in two designated regions:

1. Domain $0 \leq X \leq (r + Y)\phi_{(\tau)}$: Points remain within region 1 at both the reformation and current instants

$$(4.7a) \quad I_{1(t,\tau)} - 3 = I_{2(t,\tau)} - 3 = I_{5(t,\tau)} - 1 = 0.$$

2. Domain $(r + Y)\phi_{(\tau)} \leq X \leq (r + Y)\phi_{(t)}$: Points initially located in region 2 at the reformation instant (τ) move into region 1 at the current time (t)

$$(4.7b) \quad I_{1(t,\tau)} - 3 = I_{2(t,\tau)} - 3 = K_{5(t,\tau)} - 1 = \left[\frac{X - (r + Y)\phi_{(\tau)}}{r + Y} \right]^2.$$

3. Domain $(r + Y)\phi_{(t)} \leq X \leq L$: Points reside within the region 2 at both the reformation and current instants

$$(4.7c) \quad I_{1(t,\tau)} - 3 = I_{2(t,\tau)} - 3 = K_{5(t,\tau)} - 1 = (\phi_{(t)} - \phi_{(\tau)})^2.$$

Within these domains, the Y -coordinate varies across the thickness of the sheet, i.e., $0 \leq Y \leq H$.

5. Bending force

The principle of minimum total potential energy states that a system in equilibrium will adopt a configuration that minimizes its total potential energy functional, denoted by $\Pi(t)$. This functional represents the difference between the Helmholtz free energy (Ψ) and the work of external loads (W^{ext}), i.e. $\Pi(t) = \Psi(t) - W^{\text{ext}}(t)$. Following this principle, the displacement field, $\mathbf{u}(x, t)$, at a specific time instant (t) minimizes the total potential energy functional within the admissible set of displacement fields. This implies that any small, admissible variation of the displacement field, denoted by $\delta\mathbf{u}(x, t)$, will result in a non-negative change in the total potential energy functional for isothermal deformation of viscoelastic media. Mathematically, this variation can be expressed as:

$$(5.1) \quad \delta\Pi(t) = \delta\Psi(t) - \delta W^{\text{ext}}(t).$$

In the isothermal deformation of a viscoelastic medium, the increment of free energy is demonstrably equal to the increment of strain energy ($\Delta\Psi = \Delta W$) as shown in [35, Eq. 1.313]. Neglecting the friction force between the supporting plates and the sample surface in the bending process, the work done by the external load is equal to the product of the punch force, $P(t)$, and the variation of the punch displacement, δd . The Euler–Lagrange equation, a necessary condition for minimizing a functional, states that the functional will be minimized when the variation of the functional with respect to a specific variable (in our case, the displacement field) vanishes, namely,

$$(5.2) \quad P(t)\delta d = \frac{\partial W(t)}{\partial u_i(t)} \delta u_i.$$

Here, W represents the total strain energy, which is obtained by substituting Eqs. (4.1) and (4.7) into Eq. (2.17):

$$(5.3) \quad W(t) = \int_{\Omega_0} w(t) d\Omega_0 \\ = B \sum_{k=1}^K 3\bar{\beta}_k \left\{ [\chi_k + (1 - \chi_k) \exp(-\Gamma_k t)] \right. \\ \left. \times \int_0^H \left[\int_0^{(r+Y)\phi(t)} \left(\frac{X}{r+Y} \right)^2 dX + \int_{(r+Y)\phi(t)}^L \phi_{(t)}^2 dX \right] dY \right\}$$

$$\begin{aligned}
& + \int_0^t (\Gamma_k(1 - \chi_k) \exp[-\Gamma_k(t - \tau)t]) \\
& \quad \times \int_0^H \left[\int_{(r+Y)\phi(\tau)}^{(r+Y)\phi(t)} \left(\frac{X - (r + Y)\phi(t)}{r + Y} \right)^2 dX \right. \\
& \quad \left. + \int_{(r+Y)\phi(t)}^L (\phi(t) - \phi(\tau))^2 dX \right] dY d\tau \Big\},
\end{aligned}$$

where $\bar{\beta}_k$ is equal to $Y_{k(0,0)}(\beta_{k1} + \beta_{k2} + \beta_{k3})//3Y_{(0,0)}$. The evaluation of integrals yields:

$$\begin{aligned}
(5.4) \quad \frac{1}{B} \int_{\Omega_0} w(t) d\Omega_0 &= \sum_{k=1}^K 3\bar{\beta}_k \left\{ [\chi_k + (1 - \chi_k) \exp(-\Gamma_k t)] \phi(t)^2 \frac{1}{3} [3L - (H + 2r)\phi(t)] \right. \\
& \quad + \int_0^t (\Gamma_k(1 - \chi_k) \exp[-\Gamma_k(t - \tau)]) \frac{1}{6} (\phi(t) - \phi(\tau))^2 \\
& \quad \left. \times [6L - (H + 2r)(2\phi(t) + \phi(\tau))] d\tau \right\}.
\end{aligned}$$

Consequently, the variation of the total strain energy can be expressed as:

$$\begin{aligned}
(5.5) \quad \frac{\delta W(t)}{BH} &= \left\{ \sum_{k=1}^K 3\bar{\beta}_k \left\{ [\chi_k + (1 - \chi_k) \exp(-\Gamma_k t)] [2L - (H + 2r)\phi(t)] \phi(t) \right. \right. \\
& \quad + \int_0^t (\Gamma_k(1 - \chi_k) \exp[-\Gamma_k(t - \tau)]) \\
& \quad \left. \left. \times [2L - (H + 2r)\phi(t)] (\phi(t) - \phi(\tau)) d\tau \right\} \right\} \delta\phi.
\end{aligned}$$

Here, $\delta\phi$ represents the virtual rotation of the supporting plates induced by the virtual displacement of the punch. This relationship can be expressed using Eq. (4.2) as:

$$(5.6) \quad \delta\phi(t) = \frac{\cos^2 \phi(t)}{w - (r + a + H) \sin \phi(t)} \delta d.$$

By combining Eqs. (5.2), (5.5) and (5.6), the expression for the time-dependent bending force, $P(t)$, is obtained as follows:

$$(5.7) \quad \frac{P(t)}{BH} = \frac{2[2L - (H + 2r)\phi(t)] \cos^2 \phi(t)}{w - (r + a + H) \sin \phi(t)} \\ \times \left\{ \sum_{k=1}^K 3\bar{\beta}_k \left\{ [\chi_k + (1 - \chi_k) \exp(-\Gamma_k t)] \phi(t) \right. \right. \\ \left. \left. + \int_0^t (\Gamma_k(1 - \chi_k) \exp[-\Gamma_k(t - \tau)])(\phi(t) - \phi(\tau)) d\tau \right\} \right\}.$$

6. Results and discussion

This work presents a model of the bending process, offering a convenient procedure to determine the parameters required to describe the viscoelastic response of thermoplastic sheets reinforced with continuous fibers at the forming temperature. The model expresses the force required to bend the composite sample as a function of the bending angle and rate of deformation as well as the material parameters. Furthermore, it predicts the force required to maintain a specific bending angle in the composite sample. To validate the model's predictive capabilities, the predicted bending force is compared to previously obtained experimental measurements at various time instances. This comparison allows for the determination of the viscoelastic material parameters.

The force required to maintain a 90° bending angle after a sufficiently long time can be determined using Eq. (5.7) by letting time t approach positive infinity. This limit yields:

$$(6.1) \quad P_\infty = \lim_{t \rightarrow \infty} P(t) = K_\infty BH \sum_{k=1}^K 3\bar{\beta}_k \chi_k.$$

Here, K_∞ is a dimensionless geometric constant defined by:

$$(6.2) \quad K_\infty = \frac{\pi}{8} \frac{8L - \pi(H + 2r)}{2w - \sqrt{2}(r + a + H)}.$$

By combining Eqs. (5.7) and (6.1), we can obtain an expression for the bending force, $P(t)$, as follows:

$$(6.3) \quad \frac{P(t)}{P_\infty} = \frac{2 \cos^2 \phi(t) [2L - (H + 2r)\phi(t)]}{K_\infty [w - (r + a + H) \sin \phi(t)]} \left\{ \phi(t) \left[1 + \sum_{k=1}^K C_k \exp(-\Gamma_k t) \right] \right. \\ \left. + \int_0^t \sum_{k=1}^K (\Gamma_k C_k \exp[-\Gamma_k(t - \tau)])(\phi(t) - \phi(\tau)) d\tau \right\},$$

where C_k are given by

$$(6.4) \quad C_k = \frac{\sum_{k=1}^K \bar{\beta}_k (1 - \chi_k)}{\sum_{m=1}^K \bar{\beta}_m \chi_m}, \quad k = \{1, 2, \dots, K\}.$$

Figure 3 presents the experimentally measured bending force on a composite sample reported in [19]. The sample was bent at a constant velocity of 500 mm/min to a 90° angle and then held at that deformation until the load reached a steady-state value. The test was conducted under isothermal conditions at 180°C. The figure also compares the predicted bending loads from both a previous viscous model and the present viscoelastic model.

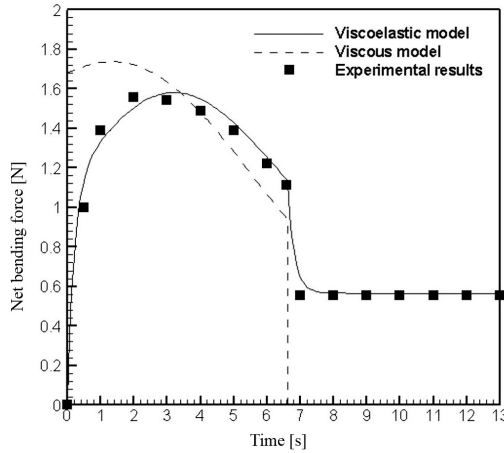


FIG. 3. Comparison of analytical functions predicting bending load with the previous experimental results [20] in different time, forming speed = 500 mm/min; temperature = 180°C.

The experimental data were obtained using Plytron samples, which are polypropylene/glass fiber composites with a nominal fiber volume fraction of 35%. Pre-consolidated laminates with a stacking sequence of $[0]_8$ were cut into sheets with 140 mm in length and 40 mm in width. The unidirectional continuous glass fibers were aligned parallel to the sample length.

The anisotropic viscoelastic model utilizes a simplified network structure, where each junction is connected by a single type of active links ($K = 1$):

$$(6.5) \quad \frac{P(t)}{P_\infty} = \frac{2 \cos^2 \phi(t) [2L - (H + 2r)\phi(t)]}{K_\infty [w - (r + a + H) \sin \phi(t)]} \times \left\{ \phi(t) [1 + C_1 \exp(-\Gamma_1 t)] + \int_0^t \Gamma_1 C_1 \exp[-\Gamma_1(t - \tau)] (\phi(t) - \phi(\tau)) d\tau \right\}.$$

Two material parameters including C_1 and Γ_1 are unknown in the Eq. (6.5) and the other variables are dependent on the initial dimension of samples (L, H), the dimension of bending die (r, a, w) and the function of bending angle. Based on the measured bending force data and the analytical function for $P(t)/P_\infty$ (Eq. (6.5)), the material parameters C_1 and Γ_1 are determined using a least-squares numerical method, resulting in values of $C_1 = 6.414$ and $\Gamma_1 = 5\text{ s}^{-1}$. Subsequently, Eq. (6.4) is used to calculate the constants associated with the active chain as:

$$(6.6) \quad \chi_1 = \frac{1}{1 + C_1} = 0.135.$$

The constants associated with the active link in the model are determined based on the experimentally measured forces reported in [18, 19] required to maintain the deformed geometry after a sufficiently long time. For the specific experimental setup employed ($H = 4\text{ mm}$, $r = a = 16\text{ mm}$), Eqs. (6.1) and (6.2) yield:

$$(6.7) \quad \bar{\beta}_1 = \frac{P_\infty}{3\chi_1 BHK_\infty} = \frac{8P_\infty}{3\pi\chi_1 BH} \frac{2w - \sqrt{2}(r + a + H)}{8L - \pi(H + 2r)} = 5923.61\text{ Pa}.$$

Figure 3 depicts the characteristic behavior of the bending force during the three-stage test. The load initially increases from zero as the bending angle progresses, reaching a maximum value before full deformation (90°) is achieved. This is followed by a gradual decrease in load as the forming process continues. The primary mechanism responsible for this load reduction is the snapping of some active links within the material. While new links may reform during bending, these reformed links do not exhibit any initial strain.

Upon completion of the 90° bending and cessation of punch movement, the force required to maintain the deformed state decreases. This force quickly reaches a steady-state value within a short period. The observed load reduction is attributed to the relaxation of stored strain energy in the snapped active links. Consequently, the only remaining stored energy in the deformed sample after a sufficiently long time originates from the permanent links. The final holding load exhibits a linear dependence on the volume fraction of these permanent links.

For comparison purposes, the bending load was also calculated using an anisotropic viscous model. This model incorporates the non-Newtonian viscous behavior of the melted resin within the composite sheets. As described in [20], the viscous model relates the load required to deform the thermoplastic composite sheets to various factors, including viscous material constants, bending angle, punch velocity and sample geometry. The bending load predicted by the viscous model, denoted by $P_{(t)}^{\text{Vis}}$, is expressed by the following equation [20]:

$$(6.8) \quad P_{(t)}^{\text{Vis}} = \frac{2Hmv[L - (r+H)\phi(t)] \cos^4 \phi(t)}{L - (r+a+H) \sin \phi(t)} \left(\frac{\cos^2 \phi(t)}{w - (r+a+H) \sin \phi(t)} \right)^{n-1},$$

where m and n are material parameters that characterize the non-Newtonian viscous behavior of the melted resin. Notably, the dependence of stress on the rate-of-deformation tensor in viscous media leads to a non-zero predicted load at the initial instant ($t = 0$), as observed in Fig. 3. This non-linear variation of the bending load in the viscous model stems from the combined effects of the resin's non-Newtonian behavior and the time-dependent strain rate during deformation. Finally, the viscous model predicts that the load reduces to zero once the deformation ceases ($t \rightarrow \infty$).

Previous studies [3, 19] have demonstrated that the response of reinforced thermoplastic sheets during forming is sensitive to the rate of deformation at the forming temperature. Selecting an appropriate forming rate can even mitigate certain defect formations. Figure 4 presents the calculated time variation of the bending load required to deform the sample at different punch velocities (50, 200, and 500 mm/min) using the viscoelastic model.

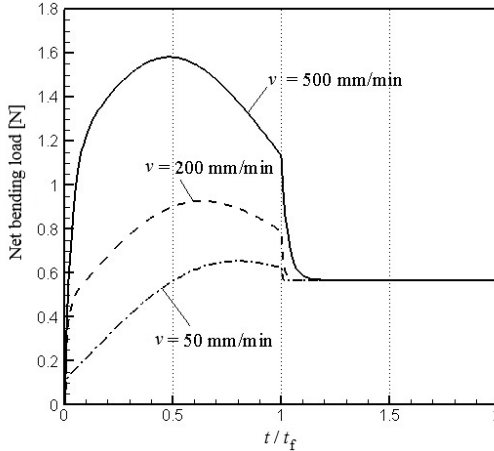


FIG. 4. Net bending load versus time in different forming speed.

To account for the significant difference in bending completion time (t_f) at these velocities, the bending load variation is plotted against the normalized time ratio (t/t_f). As the rate of deformation increases, the viscoelastic model predicts less time available for initial active link breakage, leading to a higher strain energy storage within the material at higher velocities. Consequently, as shown in Fig. 4, the bending load increases with an increasing deformation rate.

While strain energy in active links accumulates during deformation, link breakage triggers relaxation of the stored energy. Notably, at higher deformation rates, most active links possess higher strain energy due to the reduced

time for breakage. The subsequent breakage of these high-energy links significantly contributes to the observed load reduction. This explains why the load reduction occurs at a lower relative time, and the bending load reaches its peak at an earlier normalized time for faster forming processes (Fig. 4).

Finally, after deformation ceases, the bending loads for all velocities converge towards the same steady-state value. This behavior is attributed to the assumption of a constant number of permanent active links for a given temperature, regardless of the deformation rate.

Figure 5 compares the viscoelastic model predictions with experimental results reported in [20] for the variation of bending load as a function of both the bending angle and the deformation rate. The calculated force for a punch velocity of 500 mm/min exhibits good agreement with the experimental data. However, for the 50 mm/min punch velocity, the model underestimates the bending load compared to the measured values.

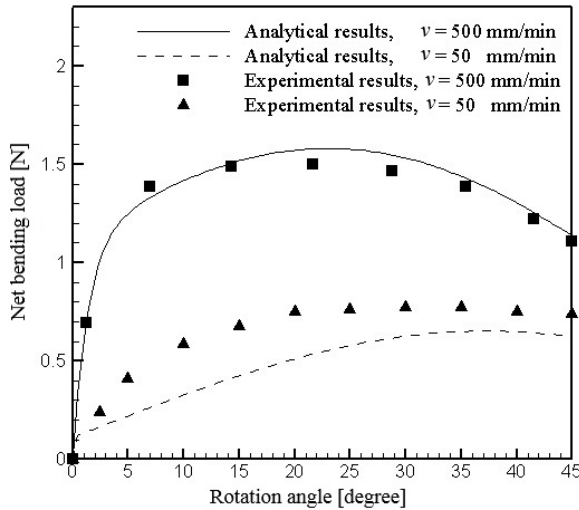


FIG. 5. The prediction of present viscoelastic model compared with experimentally measured bending load [20] in different bending angles and rates of deformation.

Previous experimental studies on the bending process [19, 33] have identified in-plane buckling of some continuous fibers as a potential contributor to the observed discrepancy. MARTIN *et al.* [19] observed that bending samples formed at a slower speed (50 mm/min) exhibited a greater wrinkling amplitude compared to those formed at a higher speed (500 mm/min). Since the phenomenon of buckling is expected to be more pronounced at lower velocities, as it allows more time for the fibers to buckle before reaching their critical stress. This energy dissipation due to fiber buckling during deformation would necessitate a higher

force to bend the sample at lower velocities. Consequently, the buckling effect could also contribute to the requirement of a greater final force to maintain the 90° bending angle in samples deformed at lower velocities.

To achieve a more accurate prediction of the bending force, future research endeavors could incorporate a post-buckling analysis into the model framework.

7. Conclusions

This work presents a viscoelastic model based on the concept of transient reversible networks to analyze the bending process of reinforced thermoplastic sheets at elevated temperatures. The strain energy at the current instant is the sum of the stored energy in the initial active links and the reformed links during the deformation process. Due to the presence of these active links, the composite material undergoing finite deformation can be considered a reinforced hyperelastic material in the continuum approach. The strain energy function of hyperelastic satisfies the criteria of objectivity, principle of material symmetry, the conditions of zero energy and zero stress in the reference configuration. This model aims to capture the viscoelastic behavior, characterized by complex stress relaxation responses, observed in diverse thermoplastic resins reinforced with continuous fibers. This work provides a closed-form solution to evaluate the time-dependent strain energy and bending force experienced by the thermoplastic composite sheets during deformation.

Comparison of the model's predictions with experimental results offers a convenient approach to determine the material parameters of the viscoelastic model at the forming temperature. These parameters include:

- The number of permanent and transient active links per unit volume in the reference configuration.
- The reformation rate of active links.
- Nonlinear elastic constants of active links.

A key advantage of this model is its ability to capture the stress relaxation phenomenon observed in experimental studies of the forming process, unlike previous viscous and elastic models. Furthermore, the present formulation allows for the evaluation of bending load under various bending angles and deformation rates.

References

1. T.-C. LIM, S. RAMAKRISHNA, *Modelling of composite sheet forming: a review*, Composites Part A: Applied Science and Manufacturing, **33**, 4, 515–537, 2002.
2. K. FRIEDRICH, M. HOU, *On stamp forming of curved and flexible geometry components from continuous glass fiber/polypropylene composites*, Composites Part A: Applied Science and Manufacturing, **29**, 3, 217–226, 1998.

3. K. FRIEDRICH, M. HOU, J. KREBS, *Thermoforming of continuous fibre/thermoplastic composite sheets*, Composite Materials Series, **11**, Elsevier, 91–162, 1997.
4. D. BRANDS, L.G. DI GENOVA, E.R. PIERIK, W.J.B. GROUVE, S. WIJSKAMP, R. AKKERMAN, *Formability experiments for unidirectional thermoplastic composites*, Key Engineering Materials, Trans Tech Publishing, 1358–1371, 2022.
5. N.A. ZANJANI, S. KALYANASUNDARAM, *Experimental and numerical studies on forming and failure behaviours of a woven self-reinforced polypropylene composite*, Advanced Composite Materials, **30**, 2, 116–130, 2021.
6. P. BOISSE, R. AKKERMAN, P. CARLONE, L. KÄRGER, S.V. LOMOV, J.A. SHERWOOD, *Advances in composite forming through 25 years of ESAFORM*, International Journal of Material Forming, **15**, 3, 39, 2022.
7. G.B. MCGUINNESS, C.M. ÓBRÁDAIGH, *Effect of preform shape on buckling of quasi-isotropic thermoplastic composite laminates during sheet forming*, Composites Manufacturing, **6**, 3–4, 269–280, 1995.
8. C.M. Ó BRÁDAIGH, G.B. MCGUINNESS, S.P. MCENTEE, *Implicit finite element modelling of composites sheet forming processes*, Composite Materials Series, **11**, Elsevier, 247–322, 1997.
9. H.R. DAGHYANI, M.T. ABADI, S. FARIBORZ, *Finite element analysis of forming flow stability in thermoplastic composite sheet forming*, Key Engineering Materials, **233–236**, 703–708, 2002.
10. T.G. ROGERS, *Rheological characterization of anisotropic materials*, Composites, **20**, 1, 21–27, 1989.
11. A.J.M. SPENCER, *Theory of fabric-reinforced viscous fluids*, Composites Part A: Applied Science and Manufacturing, **31**, 12, 1311–1321, 2000.
12. B.D. HULL, T.G. ROGERS, A.J.M. SPENCER, *Theoretical analysis of forming flows of continuous-fibre-resin systems*, Composite Materials Series, 203, 1994.
13. M.T. ABADI, H. REZA, S. FARIBORZ, *Experimental wrinkling analysis in stamp forming of continuous fiber reinforced thermoplastic sheets*, [in:] Proceedings of the 1st International Congress on Manufacturing Engineering (TICME2005), Tehran, Iran, 1–8, 2005.
14. M.T. ABADI, *Rheological characterization of continuous fiber—reinforced viscous fluid*, Journal of Non-Newtonian Fluid Mechanics, **165**, 15–16, 914–922, 2010, <https://doi.org/10.1016/j.jnnfm.2010.05.001>.
15. C.M. O’BRADAIGH, R.B. PIPES, *Finite element analysis of composite sheet-forming process*, Composites Manufacturing, **2**, 3–4, 161–170, 1991.
16. A.K. PICKETT, T. QUECKBÖRNER, P. DE LUCA, E. HAUG, *An explicit finite element solution for the forming prediction of continuous fibre-reinforced thermoplastic sheets*, Composites Manufacturing, **6**, 3–4, 237–243, 1995.
17. S.P. MCENTEE, C.M. ÓBRÁDAIGH, *Large deformation finite element modelling of single-curvature composite sheet forming with tool contact*, Composites Part A: Applied Science and Manufacturing, **29**, 1–2, 207–213, 1998.
18. M.T. ABADI, *Finite element analysis for thermoforming process of continuous fiber reinforced thermoplastic composites*, Polymer Composites, **30**, 2, 138–146, 2009, <https://doi.org/10.1002/pc.20540>.

19. T.A. MARTIN, D. BHATTACHARYYA, I.F. COLLINS, *Bending of fibre-reinforced thermo-plastic sheets*, Composites Manufacturing, **6**, 3–4, 177–187, 1995.
20. D. BHATTACHARYYA, *Composite Sheet Forming*, Elsevier, 1997.
21. G.B. MCGUINNESS, C.M. ÓBRÁDAIGH, *Development of rheological models for forming flows and picture-frame shear testing of fabric reinforced thermoplastic sheets*, Journal of Non-Newtonian Fluid Mechanics, **73**, 1–2, 1–28, 1997.
22. W.R. YU, M. ZAMPALONI, F. POURBOGHRAAT, K. CHUNG, T.J. KANG, *Sheet hydro-forming of woven FRT composites: non-orthogonal constitutive equation considering shear stiffness and undulation of woven structure*, Composite Structures, **61**, 4, 353–362, 2003.
23. J. CAO, P. XUE, X. PENG, N. KRISHNAN, *An approach in modeling the temperature effect in thermo-stamping of woven composites*, Composite Structures, **61**, 4, 413–420, 2003.
24. E. GUZMAN-MALDONADO, N. HAMILA, N. NAOUAR, G. MOULIN, P. BOISSE, *Simulation of thermoplastic prepreg thermoforming based on a visco-hyperelastic model and a thermal homogenization*, Materials Design, **93**, 431–442, 2016.
25. E. SÁNCHEZ, A. NÁJERA, O. SOTOMAYOR, *Numerical study of the viscoelastic mechanical response of polystyrene in the process of thermoforming through the generalized Maxwell model*, Materials Today Proceedings, **49**, 107–114, 2022.
26. G.A. HOLZAPFEL, T.C. GASSER, *A viscoelastic model for fiber-reinforced composites at finite strains: Continuum basis, computational aspects and applications*, Computer Methods in Applied Mechanics and Engineering, **190**, 34, 4379–4403, 2001.
27. Y. CHEN, Z. GUO, X.-L. GAO, L. DONG, Z. ZHONG, *Constitutive modeling of viscoelastic fiber-reinforced composites at finite deformations*, Mechanics of Materials, **131**, 102–112, 2019.
28. D. DÖRR, F.J. SCHIRMAIER, F. HENNING, L. KÄRGER, *A viscoelastic approach for modeling bending behavior in finite element forming simulation of continuously fiber reinforced composites*, Composites Part A: Applied Science and Manufacturing, **94**, 113–123, 2017.
29. B. NEDJAR, *An anisotropic viscoelastic fibre-matrix model at finite strains: continuum formulation and computational aspects*, Computer Methods in Applied Mechanics and Engineering, **196**, 9–12, 1745–1756, 2007.
30. I.I. TAGILTSEV, P.P. LAKTIONOV, A.V. SHUTOV, *Simulation of fiber-reinforced viscoelastic structures subjected to finite strains: multiplicative approach*, Meccanica, **53**, 3779–3794, 2018.
31. S. ROPERS, M. KARDOS, T.A. OSSWALD, *A thermo-viscoelastic approach for the characterization and modeling of the bending behavior of thermoplastic composites*, Composites Part A: Applied Science and Manufacturing, **90**, 22–32, 2016.
32. N. PYATOV, H.K. NATARAJAN, T.A. OSSWALD, *Experimental investigation of in-plane shear behaviour of thermoplastic fibre-reinforced composites under thermoforming process conditions*, Journal of Composites Science, **5**, 9, 248, 2021.
33. A. MARGOSSIAN, S. BEL, R. HINTERHOELZL, *Bending characterisation of a molten uni-directional carbon fibre reinforced thermoplastic composite using a Dynamic Mechanical Analysis system*, Composites Part A: Applied Science and Manufacturing, **77**, 154–163, 2015.

-
34. S.Q. WANG, *Transient network theory for shear-thickening fluids and physically cross-linked networks*, *Macromolecules*, **25**, 7003–7010, 1992.
 35. A.D. DROZDOV, *Mechanics of Viscoelastic Solids*, Wiley, 1998.
 36. A.D. DROZDOV, *A constitutive model in finite thermoviscoelasticity based on the concept of transient networks*, *Acta Mechanica*, **133**, 1, 13–37, 1999.
 37. J.M. BALL, *Convexity conditions and existence theorems in nonlinear elasticity*, *Archive for Rational Mechanics and Analysis*, **63**, 337–403, 1976.
 38. J. SCHRÖDER, P. NEFF, *Invariant formulation of hyperelastic transverse isotropy based on polyconvex free energy functions*, *International Journal of Solids and Structures*, **40**, 2, 401–445, 2003.
 39. M. ITSKOV, N. AKSEL, *A class of orthotropic and transversely isotropic hyperelastic constitutive models based on a polyconvex strain energy function*, *International Journal of Solids and Structures*, **41**, 14, 3833–3848, 2004.
 40. Z.Y. GUO, X.Q. PENG, B. MORAN, *A composites-based hyperelastic constitutive model for soft tissue with application to the human annulus fibrosus*, *Journal of the Mechanics and Physics of Solids*, **54**, 9, 1952–1971, 2006.
 41. K. CHAIMOON, P. CHINDAPRASIRT, *An anisotropic hyperelastic model with an application to soft tissues*, *European Journal of Mechanics-A/Solids*, **78**, 103845, 2019.
 42. J. SCHRÖDER, P. NEFF, V. EBBING, *Anisotropic polyconvex energies on the basis of crystallographic motivated structural tensors*, *Journal of the Mechanics and Physics of Solids*, **56**, 12, 3486–3506, 2008.
 43. G.A. HOLZAPFEL, T.C. GASSER, R.W. OGDEN, *A new constitutive framework for arterial wall mechanics and a comparative study of material models*, *Journal of Elasticity and the Physical Science of Solids*, **61**, 1–48, 2000.
 44. J. SCHRÖDER, P. NEFF, D. BALZANI, *A variational approach for materially stable anisotropic hyperelasticity*, *International Journal of Solids and Structures*, **42**, 15, 4352–4371, 2005.
 45. A.C. PIPKIN, T.G. ROGERS, *Plane deformations of incompressible fiber-reinforced materials*, *Journal of Applied Mechanics*, **38**, 3, 634–640, 1971.
 46. S.G. ADVANI, *Flow and rheology in polymer composites manufacturing*, S.G. Advani [ed.], *Composite Materials Series*, **10**, 1994.

Received July 6, 2024; revised version December 7, 2024.

Published online February 17, 2025.
